J IRAN CHEM SOC
DOI 10.1007/s13738-015-0715-8

ORIGINAL PAPER

Fluorophore-tagged superparamagnetic iron oxide nanoparticles as bimodal contrast agents for MR/optical imaging

Parvin Eghbali[1] · Hassan Fattahi[2] · Sophie Laurent[3,4] · Robert N. Muller[3,4] · Yones Mosaei Oskoei[2]

Received: 6 March 2015 / Accepted: 8 August 2015

Abstract A stable bimodal contrast agent for both MRI and fluorescence imaging was prepared based on fluorescent superparamagnetic iron oxide nanoparticles. In order to increase the stability of the product in a physiological medium, the designed route for preparation of this bimodal contrast agent is based on covalent linkages. Superparamagnetic magnetite nanoparticles were prepared by a coprecipitation method in polyol media, and then the surface of nanoparticles was modified with 3-aminopropyltriethoxysilane (APTES) to introduce reactive amine groups on the surface of nanoparticles. The hybrid nanoparticles were obtained by conjugating rhodamine B to APTES-modified superparamagnetic Fe_3O_4 nanoparticles through amide linkage. Longitudinal (r_1) and transverse (r_2) proton relaxivities and their ratio (r_2/r_1) obtained for bimodal contrast agent in different magnetic fields show their higher efficiency as T_2 contrast agent for MRI in comparison with commercially available magnetite-based contrast agents. Moreover, these nanoparticles can be followed up by fluorescence imaging. This study shows that rhodamine B-tagged iron oxide nanoparticles are well suited as a contrast agent for dual modality magnetic resonance and fluorescence imaging.

Keywords Dual modality imaging · Contrast agent · Molecular imaging · Iron oxide nanoparticles · MRI · Optical imaging

Introduction

Multimodality molecular imaging is now playing a pivotal role in biomedical research for noninvasive, quantitative visualization of in vivo fundamental molecular and cellular processes [1]. This combined imaging modality is an emerging technology that utilizes the strength of different modalities and yields a hybrid imaging platform with benefits superior to those of any of its individual components [2–4]. Most of the molecular imaging techniques require molecular probes capable of interacting with specific targets of the imaging technique.

Since magnetic resonance imaging (MRI) provides noninvasive, three-dimensional examination of biological events in living organisms, it is one of the most powerful diagnostic tools in modern clinical medicine [5]. Contrast in anatomical MR images is mainly due to differences in proton density and inherent differences in the relaxation times of tissue water. Relaxation times can be manipulated with the use of exogenous contrast agents [6, 7].

MRI has high spatial resolution and is able to provide detailed anatomical information, but in order to become a competitive molecular imaging modality, this technique has low sensitivity which may be realized by developing contrast agents with a very high relaxivity [8–10]. Progress in generating suitably high relaxivities has been achieved through the formulation of nanoparticulate contrast agents

✉ Hassan Fattahi
fattahi@mut.ac.ir; hassan.fattahi@gmail.com

[1] Department of Applied Chemistry, Faculty of Chemistry, University of Mahaghegh Ardabili, Ardabil, Iran

[2] North-West Institute of Science and Technology, Malek Ashtar University of Technology, Urmia, Iran

[3] Department of General, Organic and Biomedical Chemistry, NMR and Molecular Imaging Laboratory, University of Mons, Avenue Maistriau 19, 7000 Mons, Belgium

[4] Center for Microscopy and Molecular Imaging (CMMI), Rue Adrienne Bolland 8, 6041 Gosselies, Belgium

Published online: 19 August 2015

mainly including iron oxide [11–19]. Due to recent developments in the successful synthesis of more effective versions of these contrast agents, MRI is becoming an increasingly important molecular imaging technique. Significantly, multimodal MRI contrast agents have been developed that are equipped with labels for complementary imaging modalities, such as fluorescence [20–26]. Apart from using as MRI contrast agents, superparamagnetic iron oxide nanoparticles have various applications in different fields including drug delivery [27–33], gene delivery [34–36], separation [37–40], tumor treatment through hyperthermia [41], biosensing [42], and material assembly [43–46], that show the high importance of research on these nanomaterials.

Imaging tools highly complementary to MRI are optical modalities [47–49] such as confocal microscopy, intravital microscopy [50] and fluorescence imaging [26, 51–53]. These techniques allow the detection of multiple fluorescent species with high speed and sensitivity. However, the major limitation of optical imaging methods is related to the low tissue penetration depth of light and also a drawback of these optical techniques is that little anatomical information can be obtained. Therefore, the combination of MRI and optical methods would provide significant advantages [54] and can be accomplished by designing imaging probes that exhibit both magnetic and fluorescent properties. This can be realized with nanotechnology, which offers the exciting possibility of creating high efficient and targeted contrast agents that have multiple properties integrated [55, 56].

In the present study, superparamagnetic iron oxide nanoparticles were synthesized in polyol media to obtain nanoparticles with narrow size distribution. In order to introduce amino groups on the surface of nanoparticles to facilitate the further rhodamine B conjugation through amide linkage, nanoparticles were modified with 3-aminopropyltriethoxysilane (APTES). APTES is a well-known intermediate for surface modification of nanomaterials that is used in various researches [57, 58]. Finally, rhodamine B was chemically linked to the APTES-modified iron oxide nanoparticles. Different characterization methods including MRI and optical imaging of final products revealed their high potential as bimodal contrast agents for magnetic resonance and optical imaging.

Experimental

Materials

Ferric chloride solution ($FeCl_3$, 45 %), ferrous chloride tetrahydrate ($FeCl_2.4H_2O$, >99 %), sodium hydroxide, and diethyleneglycol were purchased from Fluka. 3-aminopropyltriethoxysilane (APTES), N-(3-dimethylaminopropyl)-N′-ethyl carbodiimide hydro chloride (EDC.HCl), glycerol, methanol, diisopropylethylamine (DIPEA), and ethanol were purchased from Sigma-Aldrich. All the materials mentioned above were used without further purification. Dialysis membranes (MWCO = 30,000 and 12,000) were purchased from Sigma-Aldrich (Germany).

Synthesis of magnetite nanoparticles

Magnetite nanoparticles were prepared by co-precipitation of Fe^{2+} and Fe^{3+} in polyol media according to the protocol described before [59]. Briefly, a 25 ml mixture of $FeCl_2.4H_2O$ and $FeCl_3$ (3.3 M with $[Fe^{3+}]/[Fe^{2+}]=2$) in diethyleneglycol (250 ml) was heated at 170 °C under argon protection. After 10 min, solid (pellet) NaOH (15 g) was added in order to prevent the addition of any aqueous media. The solution was stirred during 1 h at 170 °C. This mixture was then cooled to room temperature. The black gelatinous precipitate was isolated from the solution by magnetic decantation ($B_0 = 0.5$T). Finally, the precipitate was dispersed in deionized water and centrifuged at 10,000 rpm for 15 min to remove aggregates.

Preparation of APTES-modified magnetite nanoparticles

For the surface silanization reaction of the magnetite nanoparticles, a modification of Duguet's method was used [60]. A solution of methanol (10 ml) and APTES (8.4 ml) was added dropwise for 5 min to a suspension of ferrofluid (20 ml, 0.25 M) dispersed into 10 ml of methanol. After stirring at room temperature for 12 h, 20 ml of glycerol were added. Then, methanol and water were removed at 40 and 80 °C for methanol and for 2 h at 100 °C for water. Flocculated APTES-modified nanoparticles were washed three times with 40 ml of acetone. Following the addition of 40 ml of water, peptization was performed by slowly decreasing pH from 10.4 to 3 with nitric acid. The reaction mixture was magnetically stirred at this condition for 1 day, and then the pH was adjusted to 7 by sodium hydroxide solution. For further purification, the product was dispersed in distilled water and dialyzed for 4 days by changing the external water of membrane every 12 h.

Synthesis of rhodamine B-labeled magnetite nanoparticles

In order to label magnetite nanoparticles with rhodamine B as contrast agent for optical imaging, an amidation reaction was done between amine groups of APTES-modified

nanoparticles and carboxylic acid groups of Rhodamine B. Briefly, 0.1855 ml (0.1064 mmol) diisopropylethylamine was added to 0.254 g (0.0532 mmol) rhodamine B. Then 0.153 g (0.0798 mmol) EDC.HCl was added as coupling agent to the reaction mixture and mixed for some minutes. Afterwards, APTES-modified nanoparticles was added to the reaction mixture and magnetically stirred for 24 h while the reaction mixture was protected from intense light. Finally, ultrafiltration was used for purification of rhodamine B-labeled nanoparticles from excess or unreacted reactants.

Characterization techniques

The size and shape of nanoparticles were observed with a transmission electron microscope (TEM) (JEOL TEM-2100, Japan) operated at 200 kV. For TEM investigation, the nanoparticles were deposited on a copper-grid-supported perforated transparent carbon coil. The hydrodynamic sizes (d_H) were obtained with a Zetasizer Nanoseries ZEN 3600 (MALVERN, United Kingdom).

The magnetization measurements were performed on a known amount of ferrofluid using a vibrating sample magnetometer (VSM-Nuovo Molspin, Newcastle-upon-Tyne, UK). The error on a magnetization measurement was 4 %. The fitting of the Langevin function [Eq. (1)] to the magnetometric profiles provides important information such as the crystal radius (r) and the specific magnetization (M_s) [61].

$$M = M_s L(x) \tag{1}$$

where $L(x) = \coth(x) - (1/x)$ is the Langevin function and $x = \mu B_0 = k_B T$ with μ the magnetic moment of the particle, k_B the Boltzmann constant and T the absolute temperature.

Longitudinal (R_1) and transverse (R_2) relaxation rate measurements at 0.47 and 1.41 T were obtained on Minispec Mq 20 and Mq 60 spin analyzers (Bruker, Karlsruhe, Germany). The MRI experiments were performed at room temperature on a 300 MHz (7T) Bruker Biospec imaging system (Bruker, Ettlingen, Germany) equipped with a Pharmascan horizontal magnet.

The total iron concentration was determined by the measurement of the longitudinal relaxation rate R_1 according to the method previously described [61]. Briefly, the samples were mineralized by microwave digestion (MLS-1200 Mega, Milestone, Analis, Namur, Belgium) and the R_1 value of the resulting solutions was recorded at 0.47T and 37 °C which allowed determining iron concentration, using Eq. (2):

$$[\mathrm{Fe}] = (R_1^{\mathrm{sample}} - R_1^{\mathrm{diam}}) \times 0.0915 \tag{2}$$

where R_1^{diam} (s^{-1}) is the diamagnetic relaxation rate of water (0.36 s^{-1}) and 0.0915 ($s^{-1}mM^{-1}$) is the slope of the calibration curve.

The emission spectra were measured at room temperature with a convenient excitation wavelength. The samples were measured on a PerkinElmer LS 55 spectrofluorometer (PerkinElmer, USA) and a 10 mm quartz cuvette. The excitation and emission slits were set at 10 nm with the scanning rate at 1200 nm min^{-1}. Optical images were recorded using a PhotonImager from Biospace Lab (Paris, France), with excitation at 540 nm and emission at 625 nm.

Results and discussion

The original route to functionalize iron oxide nanoparticles with rhodamine B is shown in Fig. 1. Superparamagnetic iron oxide nanoparticles were prepared in polyol media to obtain nanoparticles with narrow size distribution. Figure 2 shows the PCS diagram of synthesized nanoparticles in this condition with mean hydrodynamic size of 9.9 nm. As it can be seen from this diagram, there is only one peak with narrow size distribution. APTES-modified MNPs were achieved by the silanization reaction between APTES and the hydroxyl groups on the surface of magnetite. Figure 1b shows the procedure for labeling the nanoparticles with rhodamine B. The amidation reaction was carried out at room temperature between APTES-modified nanoparticles and rhodamine B. The excess and unreacted reactants were removed through membrane filtration.

TEM image of nanoparticles (Fig. 3) shows the good monodispersity of synthesized nanoparticles. The mean diameter of nanoparticles is 9 nm, while the diameter of the nanoparticles is spread between 6.5 and 12.9 nm. The comparison of the TEM image obtained for these nanoparticles with TEM image of Fe_3O_4 nanoparticles prepared in aqueous media [16, 17] revealed that nanoparticles prepared in polyol media are spherical with narrower particle size distribution.

The PCS diagram of rhodamine B-labeled nanoparticles (Fig. 4) show that the hydrodynamic diameter of nanoparticles after modification with optical imaging probe has increased to 149.3 nm, but still the hydrodynamic size in a range that allow the nanoparticles to be used in vivo. The increase of hydrodynamic size is an indication of surface modification of magnetic Fe_3O_4 nanoparticles with rhodamine B.

The TEM image of the rhodamine B-conjugated nanoparticles is shown in Fig. 5. According to this image, the size of these modified nanoparticles is between 7.4 and 18.7 nm with mean particle diameter of 11.6 nm. As it is clear from this TEM image, the rhodamine B- labeled

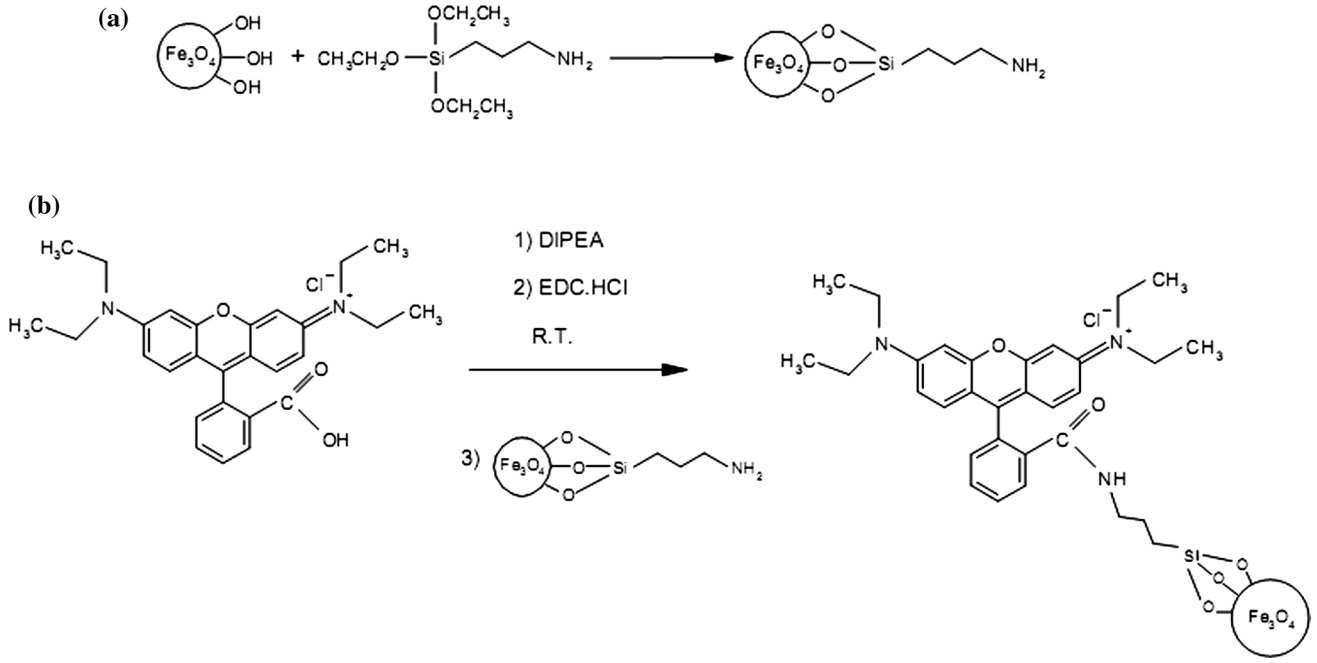

Fig. 1 **a** Surface modification of magnetic nanoparticles with APTES. **b** Conjugation of rhodamine B to APTES-modified superparamagnetic iron oxide nanoparticles

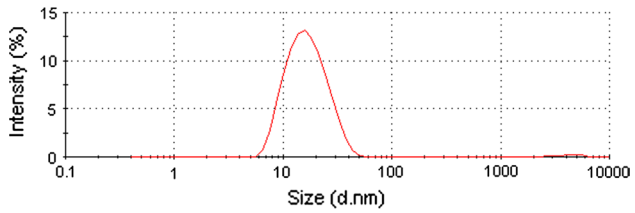

Fig. 2 Size distribution plot of Fe_3O_4 nanoparticles prepared in polyol media

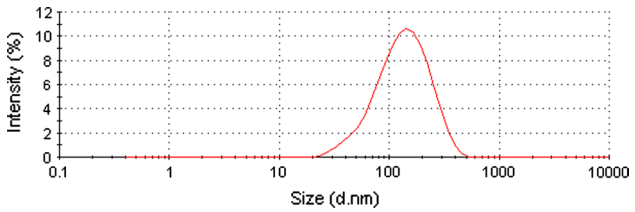

Fig. 4 Particle size distribution of rhodamine B-labeled magnetite nanoparticles

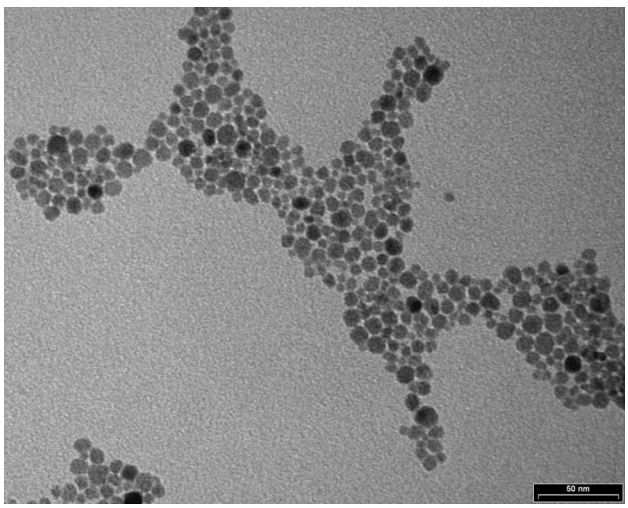

Fig. 3 TEM image of Fe_3O_4 nanoparticles prepared in polyol media

nanoparticles are completely dispersible in water without aggregation, allowing them to be used in in vivo systems.

The magnetic properties of rhodamine B-labeled Fe_3O_4 nanoparticles were measured using vibrating sample magnetometry (VSM) at room temperature (Fig. 6). As it can be seen, the curve does not display magnetic remanence and thus the nanoparticles are considered to be superparamagnetic. The magnetization saturation (M_s) of nanoparticles is about 69.2 emu/g, and the mean radius of nanoparticles obtained by this method is 4.18 nm which has a good correlation with particle diameter obtained by PCS.

The relaxation rates R_1 ($1/T_1$) and R_2 ($1/T_2$) were measured as a function of the iron molar concentration for the rhodamine B-labeled nanoparticles at 0.47 and 1.41 T in order to calculate the r_1 and r_2 relaxivities (defined as the enhancement of the relaxation rate of water protons in 1 mmol/l solution of contrast agents). The relaxivities were calculated as the slope of relaxation rate versus iron

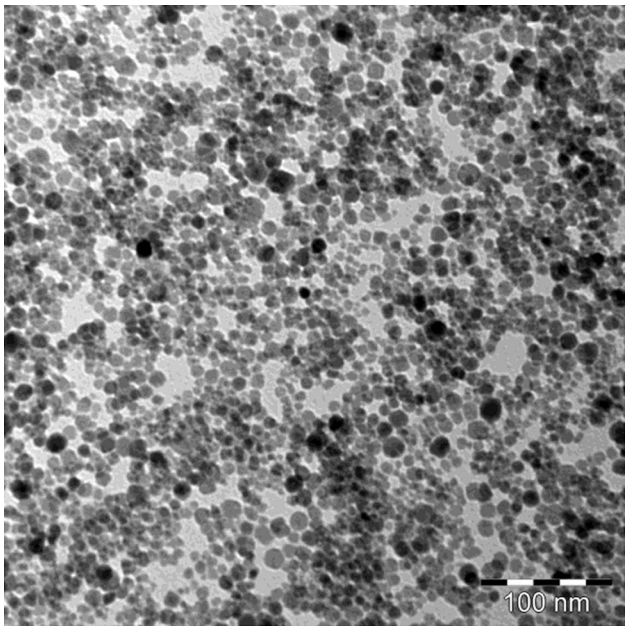

Fig. 5 TEM image of rhodamine B-conjugated iron oxide nanoparticles

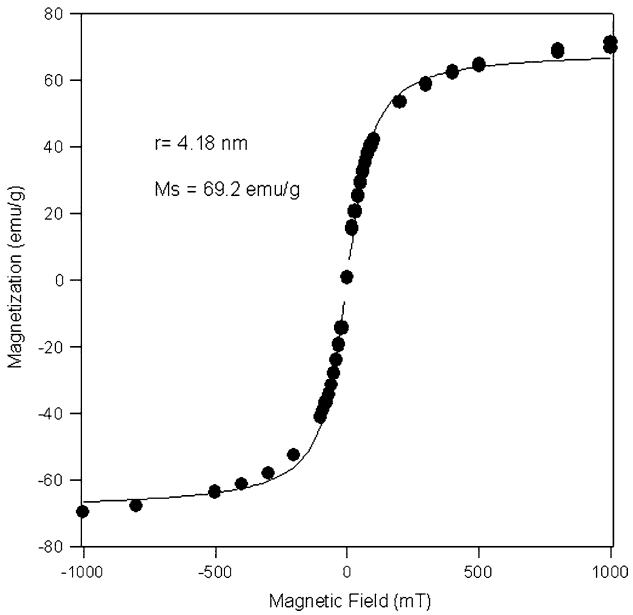

Fig. 6 Hysteresis loop measured for rhodamine B-labeled iron oxide nanoparticles

Table 1 In vitro relaxivity measurement of rhodamine B-labeled magnetic nanoparticles at 0.47 and 1.41T (at 37 °C)

Magnetic field (T)	r_1 ($mM^{-1}s^{-1}$)	r_2 ($mM^{-1}s^{-1}$)	r_2/r_1
0.47	16.93	161.21	9.52
1.41	7.22	154.84	21.45

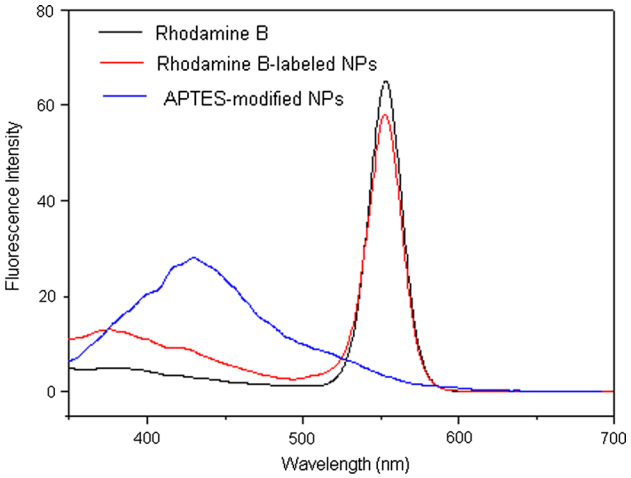

Fig. 7 Fluorescence spectra of APTES-modified nanoparticles (*blue*), rhodamine B (*black*), and rhodamine B-labeled nanoparticles (*red*)

concentration according to the Eqs. (3) and (4), respectively [62]:

$$R_1 = \frac{1}{T_1^{obs}} = r_1[\mathrm{Fe}] + \frac{1}{T_1^{diam}} \tag{3}$$

$$R_2 = \frac{1}{T_2^{obs}} = r_2[\mathrm{Fe}] + \frac{1}{T_2^{diam}} \tag{4}$$

r_1 and r_2 are the longitudinal and transversal relaxivities, respectively. T_1^{diam} and T_2^{diam} are the proton relaxation times in aqueous solutions without nanoparticles.

The r_1 and r_2 relaxivity, and r_2/r_1 ratio at different magnetic fields are summarized in Table 1. It is well known that the relaxivity ratio, r_2/r_1, is an important parameter to estimate the efficiency of T_2-contrast agents. In our work, the r_2/r_1 is calculated to be 9.52 and 21.45 at 0.47, and 1.41 T, respectively, which is much larger than that of commercially available dextran-coated nanoparticles (Endorem) (11.9 at 1.5 T) [63], demonstrating that the rhodamine B-labeled nanoparticles could perform well as T_2-contrast agents in magnetic resonance imaging.

Figure 7 shows the photoluminescence spectra of rhodamine B, APTES-modified, and rhodamine B-labeled nanoparticles. As it is clear, rhodamine B-labeled nanoparticles have the same λ_{max} as both rhodamine B and APTES-modified nanoparticles, proving the conjugation of rhodamine B to iron oxide nanoparticles.

Figure 8a shows T_2-weighted MR images of various concentrations of rhodamine B-labeled Fe_3O_4 nanoparticles in water. The MR signal intensity (related to the T_2 relaxation time in T_2-weighted images) for the samples of different concentrations is not identical. With increasing

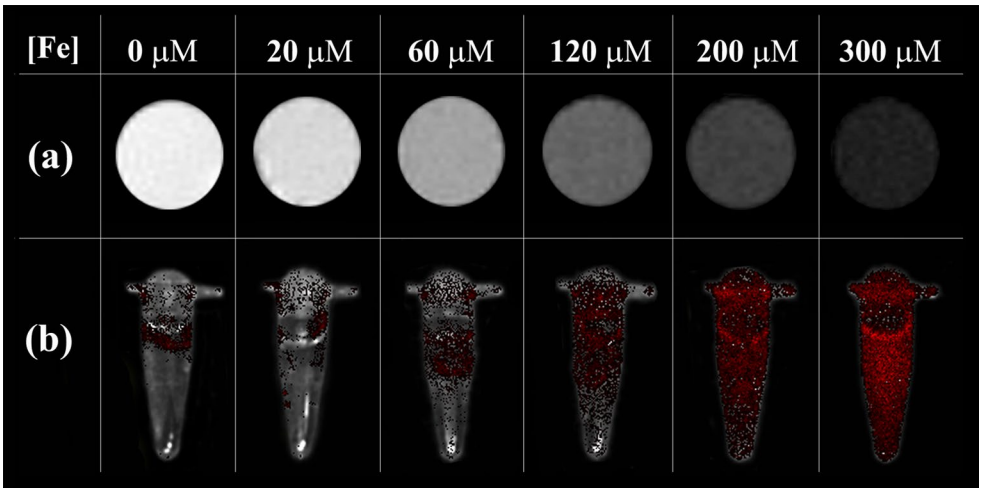

Fig. 8 **a** T_2-weighted MRI images (7T, MSME sequence: TR = 4000 ms, TE = 80 ms) of rhodamine B-labeled Fe_3O_4 nanoparticles at various iron concentrations at room temperature. **b** Optical images of rhodamine B-labeled Fe_3O_4 nanoparticles with the same iron concentration used for MRI

nanoparticle concentration, the MR signal is significantly decreased (negative contrast in T_2-weighted image). In the presence of an externally applied magnetic field, it is well known that superparamagnetic iron oxide nanoparticles create inhomogeneity in the magnetic field affecting the microenvironment, that results in dephasing of the magnetic moments of protons and hence T_2 shortening. The results indicate that the nanoparticles can generate high magnetic field gradients near the surface of the nanoparticles.

Optical images of rhodamine B-labeled nanoparticles with the same iron concentration used for MR images are shown in Fig. 8b. Rhodamine B concentration was determined by a calibration curve obtained for rhodamine B. It is clear that by increasing the rhodamine B concentration in the sample, the fluorescence intensity is increasing. Considering the optical images beside the MRI images of the same samples, reveal the high potential of rhodamine B–conjugated magnetite nanoparticles as bimodal contrast agent for MRI and optical imaging.

Conclusion

This study shows that rhodamine B-tagged iron oxide nanoparticles are well suited as contrast agent for dual modality magnetic resonance and fluorescence imaging. The superparamagnetic core induces an enhancement of the negative contrast in MRI, whereas the fluorescence imaging results from the presence of organic dyes conjugated on the surface of modified superparamagnetic nanoparticles. Because of their high transverse relaxivity and modified surface with amine functional groups, they could be very useful as a platform for further vectorization and bimodal molecular imaging purpose.

Acknowledgments This work was supported by Walloon Region (program First spin-off), Fond National de la Recherche Scientifique (FNRS), UIAP VII and ARC Programs of the French Community of Belgium. Also, the financial support of the Iranian Nanotechnology Society is gratefully acknowledged. The support and sponsorship accorded by COST Actions D38 and TD1004 are kindly acknowledged. The authors thank the Center for Microscopy and Molecular Imaging (CMMI, supported by the European Regional Development Fund and the Walloon Region).

References

1. R. Weissleder, B.D. Ross, A. Rehemetulla, S.G. Gambhir, *Molecular Imaging: Principals and Practice* (People's Medical Publishing House, Shelton, 2010), pp. 22–35
2. H. Ziadi, R. Prasad, J. Med. Phys. **34**, 122 (2009)
3. L. Marti-Bonmati, R. Sopena, P. Bartumeus, P. Sopena, Contrast Media Mol. Imaging **5**, 180 (2010)
4. C. Tu, R. Nagao, A.Y. Louie, Angew. Chem. Int. Ed. **48**, 6547 (2009)
5. P.A. Rink, *Magnetic resonance in medicine* (Wiley Blackwell, Berlin, 2003), pp. 5–17
6. S. Laurent, L. Vander Elst, R.N. Muller, in *Encyclopedia of magnetic resonance*, ed. by R.K. Harris, R. Wasylishen (Wiley, Chichester, 2007)
7. C.F.G.C. Geraldes, S. Laurent, Contrast Media Mol. Imaging **4**, 1 (2009)
8. E. Terreno, D.D. Castelli, A. Viale, S. Aime, Chem. Rev. **110**, 3019 (2010)
9. W.J. Mulder, G.J. Strijkers, G.A. van Tilborg, A.W. Griffion, K. Nicolay, NMR Biomed. **19**, 142 (2006)
10. P.M. Winter, S.D. Caruthers, S.A. Wickline, G.M. Lanza, Curr. Cardiol. Rep. **8**, 65 (2006)
11. S. Laurent, D. Forge, M. Port, A. Roch, C. Robic, L.V. Elst, R.N. Muller, Chem. Rev. **108**, 2064 (2008)

12. M. Branca, M. Marciello, M. Ciuculescu-Pradines et al., J. Magn. Magn. Mater. **377**, 348 (2015)
13. S. Laurent, J.-L. Bridot, L.V. Elst, R.N. Muller, Future Med. Chem. **2**, 427 (2010)
14. H. Fattahi, S. Laurent, F. Liu, N. Arsalani, L.V. Elst, R.N. Muller, Nanomedicine (Lond) **6**, 529 (2011)
15. F. Liu, S. Laurent, H. Fattahi, L.V. Elst, R.N. Muller, Nanomedicine (Lond) **6**, 519 (2011)
16. N. Arsalani, H. Fattahi, M. Nazarpoor, Express Polym. Lett. **4**, 329 (2010)
17. N. Arsalani, H. Fattahi, S. Laurent, C. Burtea, L.V. Elst, R.N. Muller, Contrast Media Mol. Imaging **7**, 185 (2012)
18. P. Qiu, C. Jensen, N. Charity, R. Towner, C. Mao, J. Am. Chem. Soc. **132**, 17724 (2010)
19. Z. Wang, L. Zhao, P. Yang, Z. Lv, H. Sun, Q. Jiang, Chem. Eng. J. **235**, 231 (2014)
20. J. Sloniec, M. Schnurr, C. Witte, U. Resch-Genger, L. Schroder, A. Hennig, Chem. Eur. J. **19**, 3110 (2013)
21. A. Lascialfari, P. Arosio, S. Velu, J. Mater. Chem. **22**, 20641 (2012)
22. N. Ding, Y. Lu, R.J. Lee, C. Yang, L. Huang, J. Liu, G. Xiang, Int. J. Nanomed. **6**, 2513 (2011)
23. V.S.R. Harrison, C.E. Carney, K.W. Macrenaris, T.J. Meade, Chem. Commun. **50**, 11469 (2014)
24. H. Arami, A.P. Khandhar, A. Tomitaka, E. Yu, P.W. Goodwill, S.M. Conolly, K.M. Krishnan, Biomaterials **52**, 251 (2015)
25. N. Tse, D. Kennedy, N. Kirby, B.A. Moffat, B. Muir, R. Caruso, C. Drummond, Adv. Healthcare Mater. **2**, 836 (2013)
26. A. Bianchi, S. Dufort, F. Lux, P.-Y. Fortin, N. Tassali, O. Tillement, J.-L. Coll, Y. Cremillieux, PNAS **111**, 9247 (2014)
27. M.-H. Hsiao, Q. Mu, Z.R. Stephen, C. Fang, M. Zhang, ACS Macro Lett. **4**, 403 (2015)
28. L. Zhou, B. He, F. Zhang, A.C.S. Appl, Mater. Interfaces **4**, 192 (2012)
29. N.S. Elbialy, M.M. Fathy, W.M. Khalil, Int. J. Pharm. **490**, 190 (2015)
30. M. Halupka-Bryl, M. Bednarowicz, B. Dobosz, R. Krzyminiewski, T. Zalewski, B. Wereszczynska, G. Nowaczyk, M. Jarek, Y. Nagasaki, J. Magn. Magn. Mater. **384**, 320 (2015)
31. G. Unsoy, S. Yalcin, R. Khodadust, P. Mutlu, O. Onguru, U. Gunduz, Biomed. Pharmacother. **68**, 641 (2014)
32. J. Huang, Q. Shu, L. Wang, H. Wu, A.Y. Wang, H. Mao, Biomaterials **39**, 105 (2015)
33. A. Marcu, S. Pop, F. Dumitrache, M. Mocanu, C.M. Niculite, M. Gherghiceanu, C.P. Lungu, C. Fleaca, R. Ianchis, A. Barbut, C. Grigoriu, I. Morjan, Appl. Surf. Sci. **281**, 60 (2013)
34. N. Gandra, D.-D. Wang, Y. Zhu, C. Mao, Angew. Chem. Int. Ed. **52**, 11278 (2013)
35. T.-C. Tseng, S.-H. Hsu, Biomaterials **35**, 2630 (2014)
36. B. Cao, P. Qiu, C. Mao, Microsc. Res. Tech. **76**, 936 (2013)
37. H. Xu, Z.P. Aguilar, L. Yang, M. Kuang, H. Duan, Y. Xiong, H. Wei, A. Wang, Biomaterials **32**, 9758 (2011)
38. S. Palchoudhury, J.R. Lead, Environ. Sci. Technol. **48**, 14558 (2014)
39. S. Yang, P. Zong, J. Hu, G. Sheng, Q. Wang, X. Wang, Chem. Eng. J. **214**, 376 (2013)
40. A.L. Petranovska, N.V. Abramov, S.P. Turanska, P.P. Gorbyk, A.N. Kaminskiy, N.V. Kusyak, J. Nanostruc. Chem. (2015). doi:10.1007/s40097-015-0159-9
41. P. Pradhan, J. Giri, F. Rieken et al., J. Control. Release **142**, 108 (2010)
42. K. Thandavan, S. Gandhi, N. Nesakumar, S. Sethuraman, J.B. Rayappan, U.M. Krishnan, Sens. Actuators B **215**, 166 (2015)
43. I. Dincer, O. Tozkoparan, S.V. German, A.V. Markin, O. Yildirim, G.B. Khomutov, D.A. Gorin, S.B. Venig, Y. Elerman, J. Magn. Magn. Mater. **324**, 2958 (2012)
44. Y. Ko, D. Shin, B. Koo, S.W. Lee, W.-S. Yoon, J. Cho, Nano Energy **12**, 612 (2015)
45. A. Amarjargal, L.D. Tijing, C.-H. Park, I.-T. Im, C.S. Kim, Eur. Polym. J. **49**, 3796 (2013)
46. B. Cao, Y. Zhu, L. Wang, C. Mao, Angew. Chem. Int. Ed. **52**, 11750 (2013)
47. A. Hellebust, R. Richards-Kortum, Nanomedicine (Lond) **7**, 429 (2012)
48. G.D. Luker, K.E. Luker, J. Nucl. Med. **49**, 1 (2008)
49. C. Bremer, V. Ntziachristos, R. Weissleder, Eur. Radiol. **13**, 231 (2003)
50. R.K. Jain, L.L. Munn, D. Fukumura, Nat. Rev. Cancer **2**, 266 (2002)
51. Y.F. Tan, P. Chandrasekharan et al., Biomaterials **32**, 2969 (2011)
52. L. Josephson, M.F. Kircher, U. Mahmood, Y. Tang, R. Weissleder, Bioconjugate Chem. **13**, 554 (2002)
53. V. Ntziachristos, Ann. Rev. Biomed. Eng. **8**, 1 (2006)
54. D. Sosnovik, R. Weissleder, Prog. Drug Res. **62**, 83 (2005)
55. S.M. Moghimi, A.C. Hunter, J.C. Murray, FASEB J. **19**, 311 (2005)
56. S. Akhter, I. Ahmed et al., Curr. Cancer Drug Targets **13**, 362 (2013)
57. C. Mao, F. Wang, B. Cao, Angew. Chem. Int. Ed. **51**, 6411 (2012)
58. F. Wang, S.L. Nimmo, B. Cao, C. Mao, Chem. Sci. **3**, 2639 (2012)
59. D. Forge, S. Laurent, Y. Gossuin, A. Roch, L.V. Elst, R.N. Muller, J. Magn. Magn. Mater. **323**, 410 (2011)
60. E. Duguet, S. Mornet, J. Portier, Patent FR 2855315, 2004
61. D. Forge, Y. Gossuin, A. Roch, S. Laurent, L.V. Elst, R.N. Muller, Contrast Media Mol. Imaging **5**, 126 (2010)
62. C. Burtea, S. Laurent, L.V. Elst, R.N. Muller, Handb. Exp. Pharmacol. **185**, 135 (2008)
63. B. Basly, D. Felder-Flesch, P. Perriat, C. Billotey, J. Taleb, G. Pourroy, S. Begin-Colin, Chem. Commun. **46**, 985 (2010)